Received: 14 September 2022 | Revised: 28 February 2023 | Accepted: 6 April 2023

DOI: 10.1002/jemt.24328

RESEARCH ARTICLE

MICROSCOPY RESEARCH & TECHNIQUE WILEY

Role of galectin-3 in the elastic response of radial growth phase melanoma cancer cells

Nataly Herrera-Reinoza[1] | Tharcisio Citrangulo Tortelli Junior[2] | Fernanda de Sá Teixeira[1] | Roger Chammas[2] | Maria Cecília Salvadori[1]

[1]Instituto de Física, Universidade de São Paulo, São Paulo, Brazil

[2]Instituto do Câncer do Estado de São Paulo, Faculdade de Medicina de São Paulo, São Paulo, Brazil

Correspondence
Fernanda de Sá Teixeira, Instituto de Física, Universidade de São Paulo, São Paulo, SP, Brazil.
Email: nandast@if.usp.br

Funding information
Conselho Nacional de Desenvolvimento Científico e Tecnológico

Review Editor: Alberto Diaspro

Abstract

Melanoma is originated from the malignant transformation of the melanocytes and is characterized by a high rate of invasion, the more serious stage compromising deeper layers of the skin and eventually leading to the metastasis. A high mortality due to melanoma lesion persists because most of melanoma lesions are detected in advanced stages, which decreases the chances of survival. The identification of the principal mechanics implicated in the development and progression of melanoma is essential to devise new early diagnosis strategies. Cell mechanics is related with a lot of cellular functions and processes, for instance motility, differentiation, migration and invasion. In particular, the elastic modulus (Young's modulus) is a very explored parameter to describe the cell mechanical properties; most cancer cells reported in the literature smaller elasticity modulus. In this work, we show that the elastic modulus of melanoma cells lacking galectin-3 is significantly lower than those of melanoma cells expressing galectin-3. More interestingly, the gradient of elastic modulus in cells from the nuclear region towards the cell periphery is more pronounced in shGal3 cells.

KEYWORDS
atomic force microscopy, cell mechanics, elasticity modulus, galectin-3, keratinocytes, melanoma

Research Highlights

- AFM imaging and force spectroscopy were used to investigate the morphology and elasticity properties of healthy HaCaT cells and melanoma cells WM1366, with (shSCR) and without (shGal3) expression of galectin-3.
- It is shown the effect of galectin-3 protein on the elastic properties of cells: the cells without expression of galectin-3 presents lower elastic modulus.
- By the results, we suggest here that galectin-3 could be used as an effective biomarker of malignancy in both melanoma diagnostic and prognosis.

1 | INTRODUCTION

Melanoma is the most aggressive skin neoplastic disorder. It is originated from the malignant transformation of the melanocytes, which are in the basal layer of the epidermis. Cutaneous melanoma lesions are characterized by a high rate of invasion; the first stage is known as the radial growth phase (RGP), which consists of horizontal growth and has as result a flat tumor, confined to the epidermis. In the vertical growth phase (VGP), it invades deeper layers of the skin and could lead to the metastasis (Clark et al., 1984; Herlyn et al., 1985; Liu

et al., 2021; Soo et al., 2011). High mortality due to melanoma lesion persists around the world despite efforts to improve the treatments. This is because most of melanoma lesions are detected in advanced stages, which decreases the chances of survival (Weinstein et al., 2014), caused by the lesion's resistance to therapy.

This outlook encourages the development of new effective biomarkers of malignancy in both diagnostic and prognosis; in particular, the identification of the principal mechanics implicated in the development and progression of melanoma is essential to devise new early diagnosis strategies (Cormier et al., 2015; Davis et al., 2019). In this way, changes in the expression of a variety of molecules that define the acquisition of a more invasive phenotype have been reported (Cardoso et al., 2016). Among these alterations is the progressive loss of galectin-3 (Gal-3) expression. Galectin-3 is a matricellular protein produced by a variety of cells (either normal or tumor cells) that is eventually secreted to the extracellular space (Cardoso et al., 2016; Melo et al., 2011). Upon secretion, galectin-3 may act as a lectin interacting with a variety of glycoproteins in the cellular space, such as laminins and collagens. In the presence of galectin-3, the assembly of extracellular matrix molecules is altered. In vivo, dense collagen fibers are formed in the presence of galectin-3, for example, (Oliveira et al., 2007). In addition, alterations of the adhesive and migratory behavior of tumor cells associated to Gal-3 have been reported (Ruvolo, 2016; Thijssen et al., 2015). In fact, it has been found that thin primary melanomas express more Gal-3 than benign nevus, and this behavior is lost along tumor progression, leading to a decrease of Gal-3 expression in thicker and metastatic melanoma (Brown et al., 2012; Li et al., 2013).

On the other hand, cell mechanics is related with a lot of cellular functions and processes, for instance, motility, differentiation, migration and invasion. Biological functions can suffer remarkable alterations due to changes in their physical properties. Previous studies report significant changes in the cell structure and its behavior induced by the cancer transformation (Katira et al., 2013; Mierke, 2014). Such it is well known these alterations can affect cell growth, cell-to-cell interaction and the extracellular matrix, besides inducing the reorganization of the cytoskeleton (Jinka et al., 2012; Rao & Cohen, 1991). Therefore, understanding the relationship between cancer cell mechanics and their progression has received tremendous attention in the last decade. In particular, the elastic modulus (Young's modulus) has emerged as the most explored parameter to describe the cell mechanical properties. Most cancer cells reported in the literature (Lekka et al., 1999; Pogoda et al., 2012; Sobiepanek et al., 2017) exhibit smaller elasticity modulus, that is, large deformability compared to normal cells (Nguyen et al., 2022). This behavior is useful in the cancer diagnosis, like a unique mechanical fingerprint to discriminate cancerous cells from their normal counterparts. Actually, it has already been demonstrated that cell stiffness can be a marker of the oncological process in several types of cancer (Kim et al., 2016; Lekka et al., 2012; Xu et al., 2012), showing the connection between the large deformability of the cancer cells and their invasiveness (Hochmuth, 2000). Despite the elasticity response of biological samples has been explored using different experimental techniques (Dao et al., 2003; Du et al., 2011; Hochmuth, 2000; Laurent et al., 2002; Suresh, 2007; Tanase et al., 2007), atomic force microscope (AFM) nanoindentation (Hinterdorfer & Dufrêne, 2006; Ren et al., 2021; Rosenbluth et al., 2006; Rotsch & Radmacher, 2000; Seo & Jhe, 2008; Yang et al., 2019; Zbiral et al., 2022) is considered the most powerful technique to probe the local mechanical properties of biological systems in physiological close conditions. Moreover, topographic images of the cells with high spatial resolution can be obtained.

Here, we explored the elasticity response of two cell lines, keratinocyte cells (HaCaT cell line), and the WM1366 melanoma cell line. The last one is derived from a radial growth melanoma; in this stage tumor cells still interact closely with keratinocytes, which represent the control system. In particular, the parental WM1366 cells (shSCR) along with galectin-3 silenced WM1366 cells (shGal3) (Bustos et al., 2018) were studied to compare the deformation of these cells and shed light on the mechanisms involved in the progression of cancer.

2 | EXPERIMENTAL SECTION

2.1 | Cell culture

For this study, we chose keratenocytes (HaCaT cells) and the human melanoma cell line WM1366, which have been cultured at the "Instituto do Câncer do Estado de São Paulo Octavio Frias de Oliveira" (ICESP) in São Paulo, Brazil. All cells were cultivated in DMEM (Invitrogen) medium supplemented with 10% of fetal bovine serum (FBS from Gibco), to reduce factors that could contribute to mechanical differences among them. All cultured cells were maintained in a humidified incubator with 5% CO_2 at 37°C. The culture time was set to 144 h. Gal-3 was silenced in WM1366 cells using shRNA as described in Bustos et al. (2018).

2.2 | Sample preparation for AFM measurements

HaCaT and WM1366 melanoma cells were cultured in glass coverslips of 30 mm in diameter and with a density of 10^4 cell/well. For elasticity measurements using atomic force microscopy, cells were fixed with 4% paraformaldehyde (PFA) for 15 min in PBS and were preserved in PBS with 0.01 azide at 4°C. Before AFM measurements, glass substrates (coverslips) with cells were immersed into the AFM fluid cell setup, filled with corresponding PBS, and placed on the AFM piezo-scanner.

2.3 | AFM measurements and data analysis

All AFM data presented in this study were performed at room temperature using a Bruker Multimode 8 SPM with NanoScope V controller, coupled to an optical vision system, working in liquid conditions. V-shape silicon nitride cantilevers with a four-side pyramidal tip and

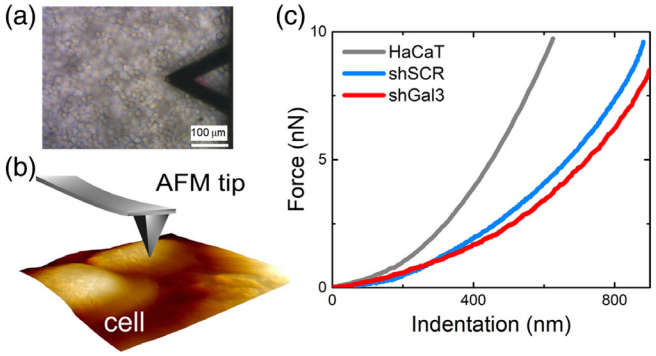

FIGURE 1 (a) Image acquired with the optical microscope coupled to the AFM, in which the cantilever and the sample can be observed; focus is on the sample. (b) Representation of the indentation of the cell using the AFM tip, the non-linear behavior can be attributed to elastic response of the cell. (c) Typical force-indentation curves at the center of the cell of HaCaT, shSCR and shGal3 cells.

half-opening angle of 35° were used as a probe (DNP-10 [Bruker] characterized by nominal spring constants of 0.12 N/m, microlevel type B). Moreover, for the WM1366 shGal3 cell line, the cantilever surface was modified by sulfur hexafluoride (SF_6) plasma treatment (Salvadori et al., 2010), to make the probe surface inert and thus preventing the melanin expressed by cells adhere to the cantilever. Before AFM measurements, cells were washed three times with sterile PBS to remove any residue that can stick to the AFM tip.

Cell topographic images were acquired in AFM contact-mode. To find the relative position of the cell to the AFM tip, an optical image is recorded such as shown in Figure 1a. To minimize cellular damage, images were acquired with a scan rate between 0.40 and 0.60 Hz and 96 points per line. The deflection sensitivity of the AFM was calibrated by taking a single force curve on the sapphire surface. The cantilever spring constant was determined by the thermal tune method (Hutter & Bechhoefer, 1993).

AFM in force spectroscopy mode was used to perform elasticity measurements. Single force curves were acquired at the cell center (see Figure 1b). These curves were obtained by approaching and retracting the cantilever of the cell surface. Cantilever deflections were recorded as a function of the relative position of the scanner during the cycle. In addition to the intrinsic mechanical response of the cell, some parameters defined during the experiment influenced the final shape of the curve, such as tip position and load forces (Ciasca et al., 2015; Krieg et al., 2019; Lekka et al., 2012; Li et al., 2008) .

In line with this, the force, *F*, was set up to 10 nN to keep the indentations on the cell within the elastic range, and the loading-unloading velocity was defined between 2 and 3 µm/s. For this study, 40 cells were tested, and 600 force curves were analyzed for each cell line. Furthermore, arrays of 32 × 32 force curves (force-volume map) collected in a 32 × 32 μm^2 area were acquired for each cell line. Since cells are highly heterogeneous, elasticity mapping would provide relevant information about diverse cellular regions, in particular, the nucleus, periphery and cell–cell junctions.

To determine the elastic modulus (*E*) of the cell, force curves were converted to force-indentation curves by identification of contact point. Force-indentation curves acquired at the center of cells are shown in Figure 1c, these data were fitted by the widely used Hertzian contact model for the four-sided pyramidal tip (Sneddon model [Sneddon, 1965]), with the assistance of AtomicJ software (Hermanowicz et al., 2014). The Hertzian model describes the indentation (δ) of a flat surface with an infinitely stiff indenter and does not consider possible adhesion forces between surfaces in contact. Therefore, considering the opening angle of the tip, θ, and the Poisson ratio, ν (typically assumed as 0.5 for cells), this system might be treated as soft incompressible material (Guz et al., 2014; Matzke et al., 2001), the fundamental relation used to calculate the elastic modulus, is given by:

$$F = \frac{1}{\sqrt{2}} \frac{E \tan\theta}{(1-\nu^2)} \delta^2,$$

2.4 | Fluorescence microscopy

10,000 cells were seeded onto a 24 well plate over a 30 mm coverslip. Cells were fixed in 4% paraformaldehyde in PBS for 15 min and washed three times with PBS. 0.2% Triton X-100 in PBS was added for 5 min for cell permeabilization. Nonspecific sites were blocked in 5% PBS/BSA for 1 h. Phalloidin-RFP was incubated in O.N. in 4°C. After three times washed in 1% PBS/BSA, cells were incubated with DAPI (0.5 mg/mL) for 1 h at room temperature in 5% PBS/BSA.

2.5 | Western blot

Cells were lysed in RIPA buffer containing protease inhibitor cocktail (Sigma-Aldrich cat: S8830) for 30 min on ice. After centrifugation (13,000 rpm for 15 min at 4°C), the protein supernatants were collected, quantified by the Bradford method (Bio-Rad, Richmond, CA) and 30 µg total proteins were separated by SDS-PAGE. Next, the proteins were transferred onto PVDF membranes, blocked with 5% non-fat dry milk for 1 h and incubated overnight with primary antibodies: M3/38 rat antiGal-3 (1:100) and β-actin (1:4000, Sigma-Aldrich AC-74). The samples were visualized with the chemiluminescent substrate ECL (GE Healthcare). Spot intensity measurement was performed using ImageJ® software.

3 | RESULTS AND DISCUSSION

3.1 | Morphological analysis of the cells

Cell surface topography images are present in Figure 2. Cellular surface information for each cell line studied is shown in the AFM height image along with their tridimensional (3D) representation, to facilitate the identification of different areas in the cell. In Figure 2a, d, a keratinocyte cell is shown. The nucleus and dendrite structures can be distinguished. In fact, the dense filamentous structures at the border of

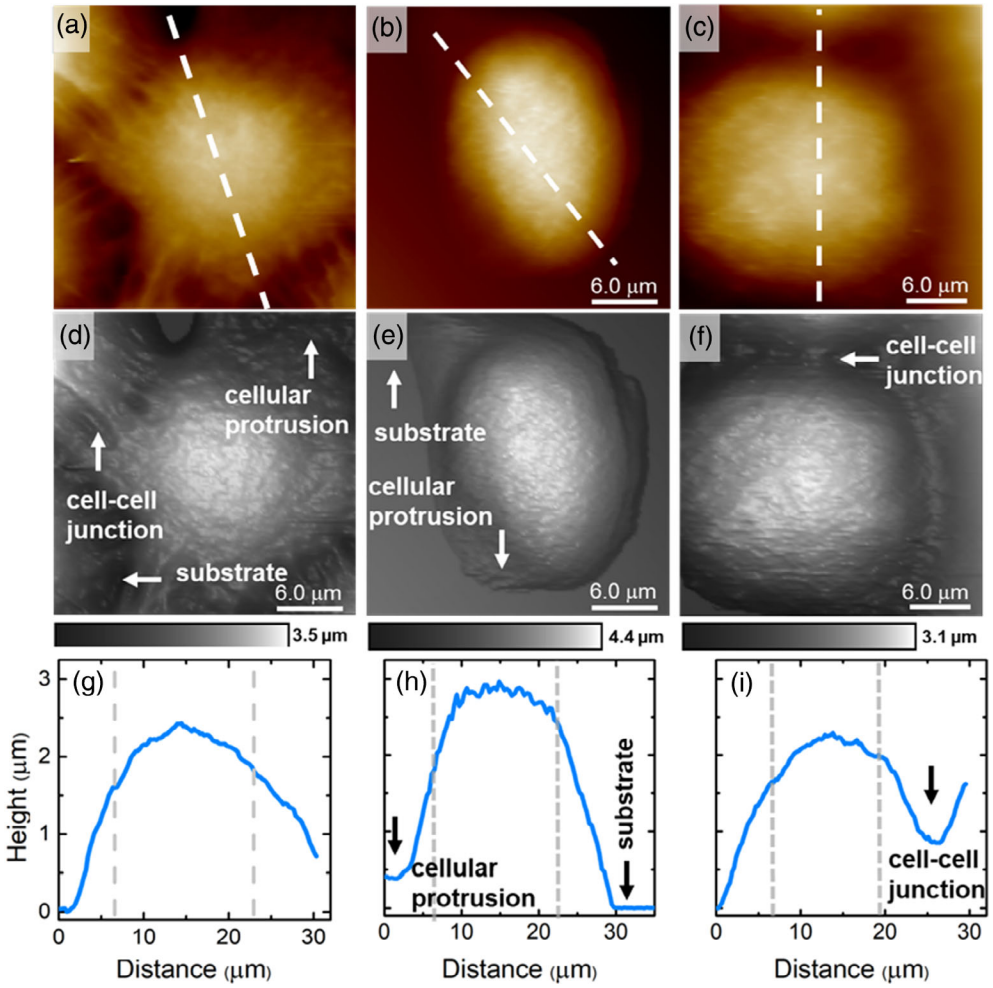

FIGURE 2 (a)–(c) AFM topography images of HaCaT, shSCR and shGal3 cells, respectively. (d)–(f) 3D representations of the images in (a)–(c). Some relevant features are pointed out in the figure, such as cell–cell junction, cellular protrusion, and the substrate where the cells are adhered. (g)–(i) The comparison of cross-section for HaCaT, shSCR, and shGal3, respectively. White dotted lines in (a)–(c) signal the cross-section on the cell.

the cell body are organized in parallel and connect adjacent keratinocytes. The coverslip substrate is poorly observed in the image due to the culture time, which induced samples in high density conditions. Unlike the keratinocyte cells, melanoma WM1366 cells showed (see Figure 2b, c, e, f) a more regular format and did not exhibit distinctive morphological features between shSCR and shGal3 cells. In addition, the cell–cell junction regions did not present filamentous structures, as it was observed for HaCaT. According to the topographic images, the fixation process by the means of crosslinking of the plasma membrane with PFA did not induce significant changes in the cellular surface, in agreement with previous studies (Guz et al., 2014). In Figures 2g–i are shown cross-sections of the cells (indicated with the white dotted line in topography images); the regions delimited by the gray dotted lines correspond to the nuclei of the cells, located in the highest part of the cells. According to the cross-sections of the cells, the height of HaCaT is similar to WM1366 cells. It is worth noting that cellular height variations due to PFA fixation have been reported (Bobrowska et al., 2016), specifically the increases in the cell height.

Such as was mentioned before, Galectin-3 expression was inhibited in WM1366 melanoma cells by shRNA as described in Bustos et al. (2018). The western blot in Figure 3 shows that the inhibition had around 80% of efficiency.

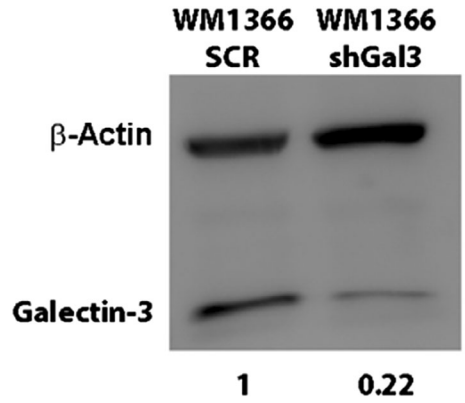

FIGURE 3 Western blot of Galectin-3 in WM1366 cells. Galectin-3 expression was reduced around 80% after shRNA transfection, compared to the scramble transfection. B-actin expression was used as load control. SCR, scramble; shGal3, shRNA to galectin-3.

3.2 | Cellular deformability of the nucleus

First works using AFM to investigate cell mechanical properties were reported by Lekka et al. (1999), who studied normal (Hu609 and

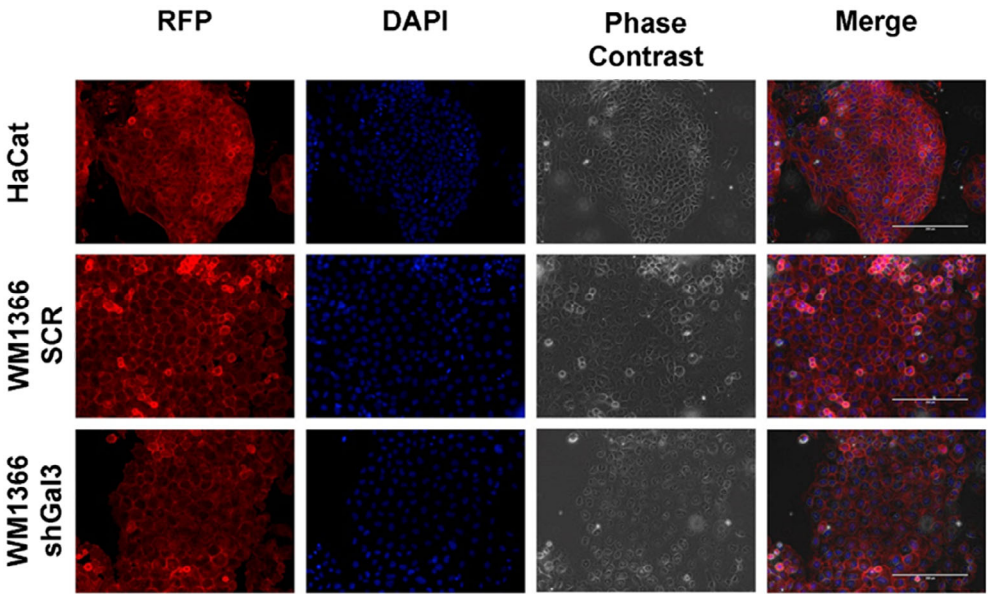

FIGURE 4
Immunofluorescence of HaCaT and WM1366 cells. Cellular distribution of phalloidin (in red) differs from the keratinocyte and the melanoma. Phalloidin is more distributed in the cytoplasm in the keratinocyte and around plasma membrane in the melanoma cell. DAPI, nuclear staining; RFP, red fluorescence protein; SCR, scramble.

HCV29) and cancerous (Hu456, T24, and BC3726) human epithelial cell lines, being found that normal cells have a Young's modulus of about one order of rigidity magnitude higher than cancerous ones. These results were attributed to poorly developed cytoskeletal elements in metastatic cells. Recently, Sobiepanek et al. (2017) studied the elastic behavior of melanocytes (HEMa-LP) and two melanoma cell types (primary RGP WM35 and metastatic A375-P melanoma cells), which were grown on glass coverslips. Topographic images did not reveal significant differences between cell lines, however it was determined that normal melanocytes have a large rigidity compared to melanoma cells. Several studies report changes in the elastic response of diverse cell lines as function of the culture density. For instance, Chiou et al. (2013) analyzed the variations of the Young's modulus for three different densities (5, 50, and 500 cells/mm^2) of MDCK cell, observing that cell elasticity increases with increasing culture density. However, other studies showed that the influence of neighboring cells on the elasticity measurements will depend on the type of cell (Pogoda et al., 2012). Zemła et al. (2018) also illustrated the influence of the culture condition on the elasticity of normal HaCaT and melanoma cells, showing that both cell culture time and culture medium composition were decisive. Meanwhile, Solon et al. (2007) demonstrated the influence of the substrate stiffness on the cytoskeleton organization and therefore in the mechanical properties. These aspects show the relative character of the elasticity modulus.

Moreover, it is well-known that the indentation depth in AFM force spectroscopy defines the cell regions that are examined. In fact, Gostek et al. (2015) used two different melanoma cell lines with similar morphology but different metastatic potential, WM115 from VGP and WM266-4 derived from metastasis to skin, to demonstrate that the elastic response depends on the indentation depth. For instance, small indentation depths provide information about cell membrane and the F-actin filaments network; while deeper indentations give details of cellular organelles, such as the cell nucleus, inclusive some authors (Bobrowska et al., 2019; Lekka, 2017; Zhao et al., 2015) associated the mechanical response of the cells in these conditions with their general elastic properties. F-actin filaments organization differs from the HaCaT cells and WM1366 cells. While is organized in the cytoplasm in the HaCaT cells, F-actin organization is around the plasma membrane in the WM1366 melanoma cells, as shown by phalloidin staining (Figure 4). In order to explore the elastic modulus in the nucleus region, single force curves, with large indentation depths in the center of each cell, were acquired (region indicated in Figure 2g–i between the gray dotted lines). Since the stiff glass substrate may induce an overestimation of the elastic modulus, indentations should not exceed 20% of the cell height (Lekka, 2017). However, to compare the elastic modulus between the cell lines studied here and to avoid substrate effects, we have used about 25% of the cell height. Figure 5 shows the histogram of elastic modulus along with box-and-whisker plots of the distributions for each cell line. Each distribution was fitted with a Gaussian function. The elastic modulus reported here corresponds to the mean value of the Gaussian function. The uncertainty was estimated from the standard deviation of the function fit and calculated with a confidence level of 95%. According to the results shown in Figure 5, keratinocytes cells exhibit more rigidity than melanoma cells, with an elastic modulus of (31.9 ± 0.4) kPa. This behavior agrees with several studies (; Lekka et al., 1999; Pogoda et al., 2012; Sobiepanek et al., 2017), which have reported more deformability in cancer cells. Moreover, for the same melanoma cell line, different deformability was found as a function of the presence or absence of galectin-3 protein. For the parental cell (shSCR) the elastic modulus found is (21.8 ± 0.5) kPa. As for the cells silenced with galectin-3 (shGal3), they are more deformable, presenting a modulus of elasticity of (16.1 ± 0.6) kPa. Although no differences were found on the cell surface by topographical measurements of AFM, it is relevant to emphasize that these cells could be distinguished by a great depth of indentation, which represents general alterations in the organization of the cytoskeleton induced by the expression of the galectin-3 protein.

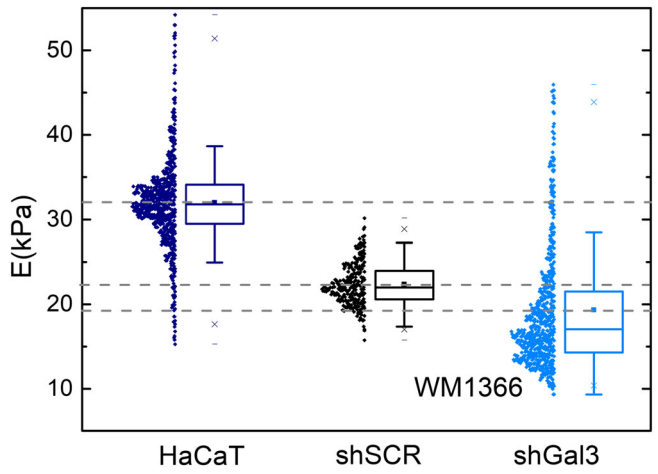

FIGURE 5 Distribution and box-and-whisker plots of the elastic modulus (*E*) for HaCaT, WM1366 shSCR and WM1366 shGal3 cells. The upper and lower whiskers represent the highest and lowest datum within 1.0 IQR (interquartile range). The median value of each distribution is also indicated by a horizontal line that goes through the box. The mean value is represented by a point inside the box, which is superimposed with the dotted line to ease the comparison of the distributions. The whiskers go from each quartile to the minimum or maximum.

3.3 | Elasticity maps

Due to the fact that elastic response of the cell is highly inhomogeneous due to the heterogeneous cytoskeleton structure, force-volume mapping, with a resolution of 32 lines/frame, was performed for each cell line. The parameters used to obtain single force curves in the center of the cells were the same for these measurements. Also, these parameters were maintained constant along the experiment. Figure 6 presents the AFM topographic images of the cells and their elastic map, which allows the directly correlation of the cellular surface with its elasticity modulus. In addition, statistical analysis of the map data, as a function of the nucleus and pericellular region of the cell along with the substrate, is shown in Figure 6. It is important to note that the map data has been separated into these three zones according to the height profile of each cell. As the nucleus height are higher, we have very reduced substrate influence. The scale used to represent the elasticity maps of the cells ranges from 10 to 100 kPa since the literature mentions that cellular systems do not exhibit stiffness values above this limit. However, in the case of shGal3, higher values of the elasticity were considered, since part of the data could be related to the substrate (glass coverslip) or

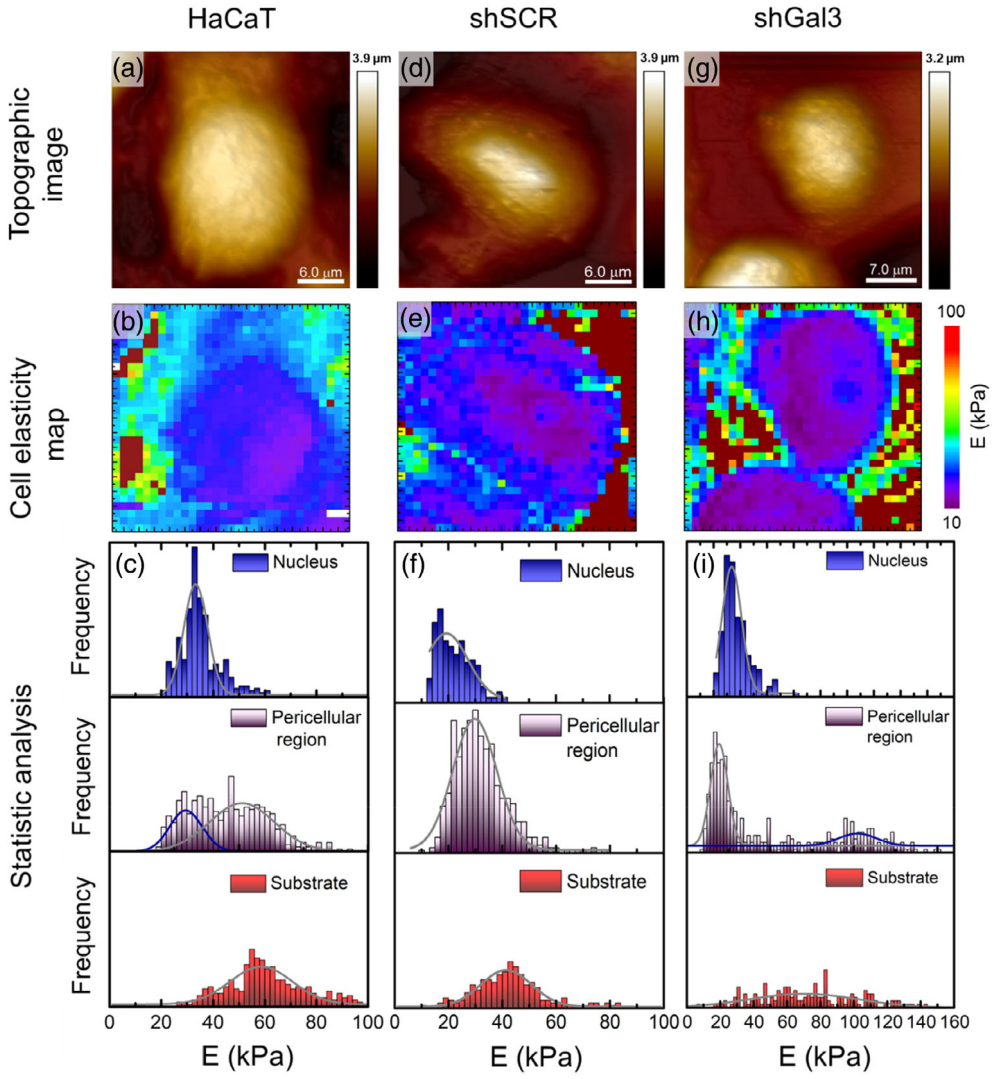

FIGURE 6 AFM topographic images, elasticity maps acquired for the region defined by the topographic images and quantitative analysis of the elastic maps for HaCaT (a)–(c), shSCR (d)–(f), and shGal3 (g)–(i) cells.

affected by the substrate, due to the thin layer of local extracellular matrix.

For the keratinocytes cells (see Figure 6a), the nucleus is clearly observed in the region with the lowest elastic modulus (as can be seen from the color scale to the right of the maps in Figure 6b). Based on the distribution in Figure 6c the nucleus average elastic modulus was (33 ± 3) kPa, which is in close agreement with the modulus found in the previous section, from the single force curve at the center of the cell. Due to a monolayer of cells in the sample, cell–cell junctions are identified in the AFM topographic image, which alters the measurement of the elastic modulus of the individual cell. This can be noticed in the histogram for the pericellular region, where it is not possible to define a unique mean value. In fact two Gaussian functions were used for the pericellular regions: for the blue curve (Figure 6c), the determined elastic modulus was (30 ± 2) kPa, while for the gray one higher elastic modulus was found (51 ± 3) kPa. As already mentioned, the measurement parameters were not readjusted during the mapping, therefore a possible substrate influence should not be discarded. For the elastic modulus distribution of the substrate was found (58 ± 3) kPa (see Figure 6c).

For the melanoma WM1366, the AFM topographic images and the elastic maps are shown in Figure 6d, e, g, h (shSCR and shGal3 respectively). The results for the cellular nucleus manifest a similar mechanical behavior to what have been observed in the study of single curves, being found $E = (20 \pm 2)$ kPa for shSCR and $E = (17 \pm 1)$ kPa for shGal3 (Figure 6f, i, respectively). In this way, the tendency of the parietal cell to be more rigid is maintained. This behavior continues in the pericellular areas, where shGal3 ($E = [19 \pm 1]$ kPa in Figure 6i) is slightly more deformable than shSCR ($E = (30 \pm 2)$ kPa in Figure 6f). Elastic modulus variations in the whole body of the shGal3 cell seem to be slighter in comparison to the parental cell. However, the map clearly reveals that the cell contour has a different module, which may not be resolved in the histogram due to the superposition of data from the substrate and cell–cell junction effects, leading to a second peak at (101 ± 4) kPa in Figure 6i.

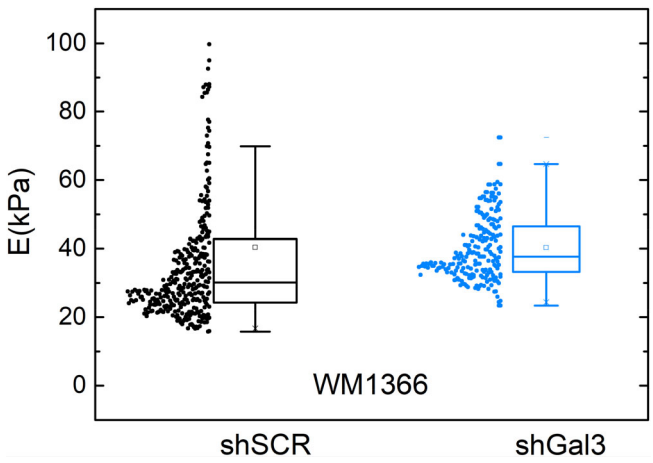

FIGURE 7 Distribution and box-and-whisker plots of the elastic modulus (*E*) at the for WM1366 shSCR and WM1366 shGal3 cells.

Substrate elastic response also showed alterations associated with the type of cell. In particular, shGal3 exhibits more stiffness ($E = [70 \pm 5]$ kPa in Figure 6i) than shSCR ($E = [41 \pm 3]$ kP in Figure 6f), which can be related to the cell migration behavior, which is a crucial process during melanoma metastasis. Indeed, some studies (Bobrowska et al., 2019) have found that cells can guide their movement by probing the substrate rigidity, leading to directed migration onto the rigid substrate. Hence, the elastic response of the substrate in the case of shGal3 can be associated with a higher migration rate.

To explore in detail the cellular periphery, avoiding the cell–cell junction region, single force analysis was performed for WM1366 cells. Figure 7 shows the result. For the shSCR cell was found a modulus of ($E = [26 \pm 2]$ kPa), which is near to the values observed in Figure 6f, that was $E = (20 \pm 2)$ kPa for the nucleus and $E = (30 \pm 2)$ kPa for the pericellular areas. However, for shGal3 the modulus was ($E = [35 \pm 2]$ kPa), in contrast with the results shown in Figure 6i, been $E = (17 \pm 1)$ kPa for the nucleus and $E = (19 \pm 1)$ kPa for the pericellular areas. Therefore, it is possible to say that the gradient of elastic modulus in cells from the nuclear region towards the cell periphery is more pronounced in cells devoid of galectin-3 than in parental cells. The increased elastic modulus in the pericellular region of cells devoid of galectin-3 suggests that the organization of the extracellular matrix in these areas was different than those observed around HaCaT and shSCR cells.

4 | CONCLUSION

We investigated, by means AFM, the morphological features and elasticity of HaCaT keratinocytes cells and the melanoma cell line WM1366 (shSCR), which expresses the endogenous lectin galectin-3 and its counterpart engineered to loose galectin-3 expression (shGal3).

We obtained topographic images in contact-mode under liquid environment (PBS) of each fixed cell line. HaCaT cells exhibit different formats and present dense filamentous structures in the cell–cell junction regions. Unlike the keratenocyte cells, melanoma WM1366 cells have a more regular format and do not show distinctive morphological features between shSCR and shGal3 cells. The cell and cell–cell junction regions do not display filamentous structures, as observed for HaCaT. Moreover, it was observed that neoplastic cells tend to overlap, which influences notoriously some morphological parameters.

The elasticity measurements made in this study indicated that the elastic modulus of melanoma cells lacking galectin-3 is significantly lower than those present in melanoma cells expressing galectin-3. More interestingly, the gradient of elastic modulus in cells from the nuclear region towards the cell periphery is more pronounced in shGal3 cells. The increased elastic module in the pericellular region of cells devoid of galectin-3 suggests that the organization of the extracellular matrix in these areas is different than those observed around HaCaT and shSCR cells. It is well known that galectin-3 may interfere with matrix assembly, as mentioned above, besides interfering with

extracellular matrix remodeling (Lagana et al., 2006; Luo et al., 2017; Takemoto et al., 2016; Vijayakumar et al., 2013).

AUTHOR CONTRIBUTIONS

Nataly Herrera-Reinoza: Investigation; writing – original draft; methodology; visualization; validation; conceptualization; formal analysis; software; writing – review and editing. **Tharcisio Citrangulo Tortelli Junior:** Conceptualization; methodology; resources. **Fernanda de Sá Teixeira:** Investigation; writing – review and editing; writing – original draft; resources; software. **Roger Chammas:** Conceptualization; investigation; funding acquisition; resources; supervision; methodology; validation; visualization. **Maria Cecília Salvadori:** Conceptualization; funding acquisition; supervision; writing – review and editing.

DATA AVAILABILITY STATEMENT

The data that support the findings of this study are available from the corresponding author upon reasonable request.

ORCID

Fernanda de Sá Teixeira https://orcid.org/0000-0002-8986-3210

REFERENCES

Bobrowska, J., Awsiuk, K., Pabijan, J., Bobrowski, P., Lekki, J., Sowa, K. M., Rysz, J., Budkowski, A., & Lekka, M. (2019). Biophysical and biochemical characteristics as complementary indicators of melanoma progression. *Analytical Chemistry*, *91*, 9885–9892. https://doi.org/10.1021/acs.analchem.9b01542

Bobrowska, J., Pabijan, J., Wiltowska-Zuber, J., Jany, B. R., Krok, F., Awsiuk, K., Rysz, J., Budkowski, A., & Lekka, M. (2016). Protocol of single cells preparation for time of flight secondary ion mass spectrometry. *Analytical Biochemistry*, *511*, 52–60. https://doi.org/10.1016/j.ab.2016.06.011

Brown, E. R., Doig, T., Anderson, N., Brenn, T., Doherty, V., Xu, Y., Bartlett, J. M. S., Smyth, J. F., & Melton, D. W. (2012). Association of galectin-3 expression with melanoma progression and prognosis. *European journal of cancer (Oxford, England: 1990)*, *48*, 865–874. https://doi.org/10.1016/j.ejca.2011.09.003

Bustos, S. O., da Silva Pereira, G. J., de Freitas Saito, R., Gil, C. D., Zanatta, D. B., Smaili, S. S., & Chammas, R. (2018). Galectin-3 sensitized melanoma cell lines to vemurafenib (PLX4032) induced cell death through prevention of autophagy. *Oncotarget*, *9*, 14567–14579. https://doi.org/10.18632/oncotarget.24516

Cardoso, A. C. F., Andrade, L. N., Bustos, S. O., & Chammas, R. (2016). Galectin-3 determines tumor cell adaptive strategies in stressed tumor microenvironments. *Frontiers in Oncology*, *6*, 127. https://doi.org/10.3389/fonc.2016.00127

Chiou, Y.-W., Lin, H.-K., Tang, M.-J., Lin, H.-H., & Yeh, M.-L. (2013). The influence of physical and physiological cues on atomic force microscopy-based cell stiffness assessment. *PLoS One*, *8*, e77384. https://doi.org/10.1371/journal.pone.0077384

Ciasca, G., Papi, M., Di Claudio, S., Chiarpotto, M., Palmieri, V., Maulucci, G., Nocca, G., Rossi, C., & De Spirito, M. (2015). Mapping viscoelastic properties of healthy and pathological red blood cells at the nanoscale level. *Nanoscale*, *7*, 17030–17037. https://doi.org/10.1039/c5nr03145a

Clark, W. H., Elder, D. E., Guerry, D., Epstein, M. N., Greene, M. H., & Van Horn, M. (1984). A study of tumor progression: The precursor lesions of superficial spreading and nodular melanoma. *Human Pathology*, *15*, 1147–1165. https://doi.org/10.1016/s0046-8177(84)80310-x

Cormier, J., Voss, R., Woods, T., Cromwell, K., & Nelson, K. (2015). Improving outcomes in patients with melanoma: Strategies to ensure an early diagnosis. *Patient Related Outcome Measures*, *229*, 229–242. https://doi.org/10.2147/PROM.S69351

Dao, M., Lim, C. T., & Suresh, S. (2003). Mechanics of the human red blood cell deformed by optical tweezers. *Journal of the Mechanics and Physics of Solids*, *51*, 2259–2280. https://doi.org/10.1016/j.jmps.2003.09.019

Davis, L. E., Shalin, S. C., & Tackett, A. J. (2019). Current state of melanoma diagnosis and treatment. *Cancer Biology & Therapy*, *20*, 1366–1379. https://doi.org/10.1080/15384047.2019.1640032

Du, G., Ravetto, A., Fang, Q., & den Toonder, J. M. J. (2011). Cell types can be distinguished by measuring their viscoelastic recovery times using a micro-fluidic device. *Biomedical Microdevices*, *13*, 29–40. https://doi.org/10.1007/s10544-010-9468-4

Gostek, J., Prauzner-Bechcicki, S., Nimmervoll, B., Mayr, K., Pabijan, J., Hinterdorfer, P., Chtcheglova, L. A., & Lekka, M. (2015). Nanocharacterization of two closely related melanoma cell lines with different metastatic potential. *European Biophysics Journal*, *44*, 49–55. https://doi.org/10.1007/s00249-014-1000-y

Guz, N., Dokukin, M., Kalaparthi, V., & Sokolov, I. (2014). If cell mechanics can be described by elastic modulus: Study of different models and probes used in indentation experiments. *Biophysical Journal*, *107*, 564–575. https://doi.org/10.1016/j.bpj.2014.06.033

Herlyn, M., Thurin, J., Balaban, G., Bennicelli, J. L., Herlyn, D., Elder, D. E., Bondi, E., Guerry, D., Nowell, P., & Clark, W. H. (1985). Characteristics of cultured human melanocytes isolated from different stages of tumor progression. *Cancer Research*, *45*, 5670–5676.

Hermanowicz, P., Sarna, M., Burda, K., & Gabryś, H. (2014). AtomicJ: An open source software for analysis of force curves. *The Review of Scientific Instruments*, *85*, 63703. https://doi.org/10.1063/1.4881683

Hinterdorfer, P., & Dufrêne, Y. F. (2006). Detection and localization of single molecular recognition events using atomic force microscopy. *Nature Methods*, *3*, 347–355. https://doi.org/10.1038/nmeth871

Hochmuth, R. M. (2000). Micropipette aspiration of living cells. *Journal of Biomechanics*, *33*, 15–22. https://doi.org/10.1016/S0021-9290(99)00175-X

Hutter, J. L., & Bechhoefer, J. (1993). Calibration of atomic-force microscope tips. *The Review of Scientific Instruments*, *64*, 1868–1873. https://doi.org/10.1063/1.1143970

Jinka, R., Kapoor, R., Sistla, P. G., Raj, T. A., & Pande, G. (2012). Alterations in cell-extracellular matrix interactions during progression of cancers. *International Journal of Cell Biology*, *2012*, 1–8. https://doi.org/10.1155/2012/219196

Katira, P., Bonnecaze, R. T., & Zaman, M. H. (2013). Modeling the mechanics of cancer: Effect of changes in cellular and extra-cellular mechanical properties. *Frontiers in Oncology*, *3*, 1–4. https://doi.org/10.3389/fonc.2013.00145

Kim, T.-H., Gill, N. K., Nyberg, K. D., Nguyen, A. V., Hohlbauch, S. V., Geisse, N. A., Nowell, C. J., Sloan, E. K., & Rowat, A. C. (2016). Cancer cells become less deformable and more invasive with activation of β-adrenergic signaling. *Journal of Cell Science*, *129*, 4563–4575. https://doi.org/10.1242/jcs.194803

Krieg, M., Fläschner, G., Alsteens, D., Gaub, B. M., Roos, W. H., Wuite, G. J. L., Gaub, H. E., Gerber, C., Dufrêne, Y. F., & Müller, D. J. (2019). Atomic force microscopy-based mechanobiology. *Nature Reviews Physics*, *1*, 41–57. https://doi.org/10.1038/s42254-018-0001-7

Lagana, A., Goetz, J. G., Cheung, P., Raz, A., Dennis, J. W., & Nabi, I. R. (2006). Galectin binding to Mgat5-modified N-glycans regulates fibronectin matrix remodeling in tumor cells. *Molecular and Cellular Biology*, *26*, 3181–3193. https://doi.org/10.1128/MCB.26.8.3181-3193.2006

Laurent, V. M., Hénon, S., Planus, E., Fodil, R., Balland, M., Isabey, D., & Gallet, F. (2002). Assessment of mechanical properties of adherent living cells by bead micromanipulation: Comparison of magnetic twisting

cytometry vs optical tweezers. *Journal of Biomechanical Engineering*, *124*, 408–421. https://doi.org/10.1115/1.1485285

Lekka, M. (2017). *Cellular analysis by atomic force microscopy* (1st ed.). Jenny Stanford Publishing. https://doi.org/10.1201/9781315364803

Lekka, M., Gil, D., Pogoda, K., Dulińska-Litewka, J., Jach, R., Gostek, J., Klymenko, O., Prauzner-Bechcicki, S., Stachura, Z., Wiltowska-Zuber, J., Okoń, K., & Laidler, P. (2012). Cancer cell detection in tissue sections using AFM. *Archives of Biochemistry and Biophysics*, *518*, 151–156. https://doi.org/10.1016/j.abb.2011.12.013

Lekka, M., Laidler, P., Gil, D., Lekki, J., Stachura, Z., & Hrynkiewicz, A. Z. (1999). Elasticity of normal and cancerous human bladder cells studied by scanning force microscopy. *European Biophysics Journal*, *28*, 312–316. https://doi.org/10.1007/s002490050213

Li, Q. S., Lee, G. Y. H., Ong, C. N., & Lim, C. T. (2008). AFM indentation study of breast cancer cells. *Biochemical and Biophysical Research Communications*, *374*, 609–613. https://doi.org/10.1016/j.bbrc.2008.07.078

Li, Z., Wang, Y., Xue, W., Si, L., Cui, C., Cao, D., Zhou, L.-X., Guo, J., & Lu, A. (2013). Expression and prognostic significance of galectin-1 and galectin-3 in benign nevi and melanomas. *Zhonghua Bing Li Xue Za Zhi*, *42*, 801–805.

Liu, D., Lin, J.-R., Robitschek, E. J., Kasumova, G. G., Heyde, A., Shi, A., Kraya, A., Zhang, G., Moll, T., Frederick, D. T., Chen, Y.-A., Wang, S., Schapiro, D., Ho, L.-L., Bi, K., Sahu, A., Mei, S., Miao, B., Sharova, T., … Boland, G. M. (2021). Evolution of delayed resistance to immunotherapy in a melanoma responder. *Nature Medicine*, *27*, 985–992. https://doi.org/10.1038/s41591-021-01331-8

Luo, H., Liu, B., Zhao, L., He, J., Li, T., Zha, L., Li, X., Qi, Q., Liu, Y., & Yu, Z. (2017). Galectin-3 mediates pulmonary vascular remodeling in hypoxia-induced pulmonary arterial hypertension. *Journal of the American Society of Hypertension*, *11*, 673–683.e3. https://doi.org/10.1016/j.jash.2017.07.009

Matzke, R., Jacobson, K., & Radmacher, M. (2001). Direct, high-resolution measurement of furrow stiffening during division of adherent cells. *Nature Cell Biology*, *3*, 607–610. https://doi.org/10.1038/35078583

Melo, F. H. M., Butera, D., Junqueira, M. d. S., Hsu, D. K., da Silva, A. M. M., Liu, F.-T., Santos, M. F., & Chammas, R. (2011). The promigratory activity of the matricellular protein galectin-3 depends on the activation of PI-3 kinase. *PLoS One*, *6*, e29313. https://doi.org/10.1371/journal.pone.0029313

Mierke, C. T. (2014). The fundamental role of mechanical properties in the progression of cancer disease and inflammation. *Reports on Progress in Physics*, *77*, 76602. https://doi.org/10.1088/0034-4885/77/7/076602

Nguyen, H. L., Man, V. H., Li, M. S., Derreumaux, P., Wang, J., & Nguyen, P. H. (2022). Elastic moduli of normal and cancer cell membranes revealed by molecular dynamics simulations. *Physical Chemistry Chemical Physics*, *24*, 6225–6237. https://doi.org/10.1039/D1CP04836H

Oliveira, F. L., Frazão, P., Chammas, R., Hsu, D. K., Liu, F. T., Borojevic, R., Takiya, C. M., & El-Cheikh, M. C. (2007). Kinetics of mobilization and differentiation of lymphohematopoietic cells during experimental murine schistosomiasis in galectin-3 −/− mice. *Journal of Leukocyte Biology*, *82*, 300–310. https://doi.org/10.1189/jlb.1206747

Pogoda, K., Jaczewska, J., Wiltowska-Zuber, J., Klymenko, O., Zuber, K., Fornal, M., & Lekka, M. (2012). Depth-sensing analysis of cytoskeleton organization based on AFM data. *European Biophysics Journal*, *41*, 79–87. https://doi.org/10.1007/s00249-011-0761-9

Rao, K. M., & Cohen, H. J. (1991). Actin cytoskeletal network in aging and cancer. *Mutation Research*, *256*, 139–148. https://doi.org/10.1016/0921-8734(91)90007-x

Ren, K., Gao, J., & Han, D. (2021). AFM force relaxation curve reveals that the decrease of membrane tension is the essential reason for the softening of cancer cells. *Frontiers in Cell and Development Biology*, *9*, 663021. https://doi.org/10.3389/fcell.2021.663021

Rosenbluth, M. J., Lam, W. A., & Fletcher, D. A. (2006). Force microscopy of nonadherent cells: A comparison of leukemia cell deformability. *Biophysical Journal*, *90*, 2994–3003. https://doi.org/10.1529/biophysj.105.067496

Rotsch, C., & Radmacher, M. (2000). Drug-induced changes of cytoskeletal structure and mechanics in fibroblasts: An atomic force microscopy study. *Biophysical Journal*, *78*, 520–535. https://doi.org/10.1016/S0006-3495(00)76614-8

Ruvolo, P. P. (2016). Galectin 3 as a guardian of the tumor microenvironment. *Biochimica et Biophysica Acta*, *1863*, 427–437. https://doi.org/10.1016/j.bbamcr.2015.08.008

Salvadori, M. C., Araújo, W. W. R., Teixeira, F. S., Cattani, M., Pasquarelli, A., Oks, E. M., & Brown, I. G. (2010). Termination of diamond surfaces with hydrogen, oxygen and fluorine using a small, simple plasma gun. *Diamond and Related Materials*, *19*, 324–328. https://doi.org/10.1016/j.diamond.2010.01.002

Seo, Y., & Jhe, W. (2008). Atomic force microscopy and spectroscopy. *Reports on Progress in Physics*, *71*, 16101. https://doi.org/10.1088/0034-4885/71/1/016101

Sneddon, I. N. (1965). The relation between load and penetration in the axisymmetric boussinesq problem for a punch of arbitrary profile. *International Journal of Engineering Science*, *3*, 47–57. https://doi.org/10.1016/0020-7225(65)90019-4

Sobiepanek, A., Milner-Krawczyk, M., Lekka, M., & Kobiela, T. (2017). AFM and QCM-D as tools for the distinction of melanoma cells with a different metastatic potential. *Biosensors & Bioelectronics*, *93*, 274–281. https://doi.org/10.1016/j.bios.2016.08.088

Solon, J., Levental, I., Sengupta, K., Georges, P. C., & Janmey, P. A. (2007). Fibroblast adaptation and stiffness matching to soft elastic substrates. *Biophysical Journal*, *93*, 4453–4461. https://doi.org/10.1529/biophysj.106.101386

Soo, J. K., Mackenzie Ross, A. D., Kallenberg, D. M., Milagre, C., Heung Chong, W., Chow, J., Hill, L., Hoare, S., Collinson, R. S., Hossain, M., Keith, W. N., Marais, R., & Bennett, D. C. (2011). Malignancy without immortality? Cellular immortalization as a possible late event in melanoma progression. *Pigment Cell & Melanoma Research*, *24*, 490–503. https://doi.org/10.1111/j.1755-148X.2011.00850.x

Suresh, S. (2007). Biomechanics and biophysics of cancer cells. *Acta Biomaterialia*, *3*, 413–438. https://doi.org/10.1016/j.actbio.2007.04.002

Takemoto, Y., Ramirez, R. J., Yokokawa, M., Kaur, K., Ponce-Balbuena, D., Sinno, M. C., Willis, B. C., Ghanbari, H., Ennis, S. R., Guerrero-Serna, G., Henzi, B. C., Latchamsetty, R., Ramos-Mondragon, R., Musa, H., Martins, R. P., Pandit, S. V., Noujaim, S. F., Crawford, T., Jongnarangsin, K., … Jalife, J. (2016). Galectin-3 regulates atrial fibrillation remodeling and predicts catheter ablation outcomes. *JACC: Basic to Translational Science*, *1*, 143–154. https://doi.org/10.1016/j.jacbts.2016.03.003

Tanase, M., Biais, N., & Sheetz, M. (2007). Magnetic tweezers in cell biology. *Methods in Cell Biology*, *83*, 473–493. https://doi.org/10.1016/S0091-679X(07)83020-2

Thijssen, V. L., Heusschen, R., Caers, J., & Griffioen, A. W. (2015). Galectin expression in cancer diagnosis and prognosis: A systematic review. *Biochimica et Biophysica Acta*, *1855*, 235–247. https://doi.org/10.1016/j.bbcan.2015.03.003

Vijayakumar, S., Peng, H., & Schwartz, G. J. (2013). Galectin-3 mediates oligomerization of secreted hensin using its carbohydrate-recognition domain. *American Journal of Physiology-Renal Physiology*, *305*, F90–F99. https://doi.org/10.1152/ajprenal.00498.2012

Weinstein, D., Leininger, J., Hamby, C., & Safai, B. (2014). Diagnostic and prognostic biomarkers in melanoma. *The Journal of Clinical and Aesthetic Dermatology*, *7*, 13–24.

Xu, W., Mezencev, R., Kim, B., Wang, L., McDonald, J., & Sulchek, T. (2012). Cell stiffness is a biomarker of the metastatic potential of ovarian cancer cells. *PLoS One*, *7*, e46609. https://doi.org/10.1371/journal.pone.0046609

Yang, Y., Xiao, X., Peng, Y., Yang, C., Wu, S., Liu, Y., Yue, T., Pu, H., Liu, N., & Jiang, H. (2019). The comparison between force volume and peakforce quantitative nanomechanical mode of atomic force microscope in detecting cell's mechanical properties. *Microscopy Research and Technique*, *82*, 1843–1851. https://doi.org/10.1002/jemt.23351

Zbiral, B., Weber, A., & Toca-Herrera, J. L. (2022). Measuring mechanical properties of breast cancer cells with atomic force microscopy. In M. Vivanco (Ed.), *Mammary stem cells, methods in molecular biology* (pp. 323–343). Springer US. https://doi.org/10.1007/978-1-0716-2193-6_19

Zemła, J., Danilkiewicz, J., Orzechowska, B., Pabijan, J., Seweryn, S., & Lekka, M. (2018). Atomic force microscopy as a tool for assessing the cellular elasticity and adhesiveness to identify cancer cells and tissues. *Seminars in Cell & Developmental Biology*, *73*, 115–124. https://doi.org/10.1016/j.semcdb.2017.06.029

Zhao, X., Zhong, Y., Ye, T., Wang, D., & Mao, B. (2015). Discrimination between cervical cancer cells and Normal cervical cells based on longitudinal elasticity using atomic force microscopy. *Nanoscale Research Letters*, *10*, 482. https://doi.org/10.1186/s11671-015-1174-y

How to cite this article: Herrera-Reinoza, N., Tortelli Junior, T. C., Teixeira, F. S., Chammas, R., & Salvadori, M. C. (2023). Role of galectin-3 in the elastic response of radial growth phase melanoma cancer cells. *Microscopy Research and Technique*, 1–10. https://doi.org/10.1002/jemt.24328